

Chapter 5

Micellar Structure of Block Copolymers in an LC Solvent

Much of the work in this chapter represents the combined efforts both of myself and of Neal Scruggs. We acknowledge the support of Dr. Jyotsana Lal and Ed Lang in designing and conducting the neutron scattering experiments. In addition, Dr. Michael Kempe and Zuleikha Kurji provided assistance in carrying out the neutron scattering experiments during separate trips to Argonne National Laboratory. Finally, the work in this chapter could not have been done without materials obtained from Dr. David Uhrig of the Macromolecular Complex Systems group at Oak Ridge National Laboratory. They provided most of the polystyrene-polybutadiene diblock copolymers used for this study.

5.1 Abstract

Block copolymers comprised of polystyrene (PS) segments and side-group liquid crystal polymer (SGLCP) segments self-assemble when mixed in a nematic liquid crystal (LC) solvent to form LC gels. We investigate a series of diblock PS-SGLCP and triblock PS-SGLCP-PS copolymer gels by small-angle neutron scattering (SANS) and rheometry. These studies show that the LC order of the host solvent imparts unique properties to the micellar gels. The micelles and intermicellar network inherit the anisotropy of the host solvent, and dramatic structural and rheological changes occur across the T_{NI} , due to a changing solvent selectivity. SANS shows that the micelles are disordered, and the micelles decrease in size with temperature. The microphase separation temperature T_{MST}

can be coincident with or higher than the T_{NI} depending on the copolymer block lengths. Rheometry reveals that both diblock and triblock copolymer mixtures can exhibit solid-like properties, depending on the PS and SGLCP block lengths. Both SANS and rheometry show that the driving force for self-assembly is increased with the PS block size: a larger PS block size results in a higher T_{MST} and a higher sol-gel transition temperature. The block copolymer micelles have a “hairy” structure with extended SGLCP coronas, small PS cores swollen with 5CB, and a soft intermicellar potential.

5.2 Introduction

Block copolymers are comprised of chemically distinct polymers covalently linked together. When a block copolymer is dissolved in a solvent that preferentially solvates one block, the block copolymers oftentimes assemble into aggregates known as micelles, and this dramatically alters the rheological properties of the solution. Unlike liquids, a micellar suspension can have a finite yield stress, but it can also coat a surface or fill a container. This type of behavior that is neither purely liquid-like or purely solid-like is termed viscoelastic, and these types of materials have wide-ranging practical interest. Block copolymer additives are used regularly in the cosmetics industry, and potential uses include their addition to jet fuels to prevent droplet formation [1] and as hydrogels to form scaffolds for tissue regeneration [2].

Block copolymers can also be combined with LC order for use in functional materials. We have demonstrated that triblock copolymers composed of a side-group LC polymer (SGLCP) mid-block and non-mesomorphic polystyrene (PS) endblocks can form LC gels when mixed with a small molecule liquid crystal (Chapter 2). In this study, we investigate the structure of the LC copolymers in the small molecule LC 4-pentyl-4'-cyanobiphenyl (5CB). PS is insoluble in nematic 5CB due to the entropic penalty of dissolving an isotropic polymer in a liquid crystal phase [3], resulting in self-assembly of the triblock copolymers to form an LC gel. We study a series of SGLCP-PS diblock and PS-SGLCP-PS triblock copolymers with different block lengths by SANS and rheometry. An interesting property of the gels is that they undergo a nematic-to-isotropic transition near 35

°C. Therefore, the nematic-to-isotropic transition of the solvent is expected to result in significant changes to the self-assembled micellar structure. Both SANS and rheometry reveal significant structural changes with temperature across the T_{NI} . Also, the PS block length is a significant parameter for the phase behavior of the gels, and samples with large (> 100 kg/mol) PS blocks form gels even above the T_{NI} .

5.3 Experimental

5.3.1 Preparation of nematic gels

The synthesis and characterization of the LC homopolymers and copolymers and the preparation of the LC gels was carried out as described in Chapter 2. The diblock and triblock PS-SGLCP copolymers are named by the size of the SGLCP block, the size of the PS block, and the polymer architecture (“AB” for diblock, “ABA” for triblock, and “LCP” for SGLCP homopolymer), as shown in Table 5.1. The homopolymers, triblock prepolymers, and diblock prepolymer for 890(70)AB and 840(190) AB were purchased and used as received from Polymer Source. All the other diblock prepolymers were obtained from the Macromolecular Complex Systems group from Oak Ridge National Labs and used as received.

5.3.2 LC phase identification

The transition temperatures of the LC gels were determined using a Zeiss polarized optical microscope (POM) with a Mettler FP82 hot stage. The temperature was slowly raised at 1 °C/min, and the phases were identified along with the temperature at which phase transitions began. Some samples exhibited a biphasic region in between single-phase isotropic and single-phase nematic mixtures. The T_{NI} was taken to be the onset temperature of the biphasic region.

5.3.3 Rheometry

Rheometry was performed on a TA Instruments ARES-RFS rheometer equipped with a 25 mm diameter titanium shear cell. Except where otherwise noted, rheometry was performed in a cone-and-plate geometry having a 0.0202 radian cone angle. All experiments were performed in the linear regime as verified by dynamic strain sweeps.

5.3.4 SANS

SANS experiments were performed on the small-angle scattering instrument (SASI) at the Intense Pulsed Neutron Source at Argonne National Laboratory. Diblock and triblock copolymer samples were mixed with perdeuterated 5CB (D5CB) [4] at concentrations of 5 and 10 wt %. The samples were loaded into 1 mm-thick quartz cells, except where otherwise noted, and the cells were placed in a temperature-controlled sample holder. The scattering experiments were performed on polydomain samples at temperatures ranging between 25 °C and 60 °C. Polydomain samples can be azimuthally averaged and therefore have a much better signal to noise ratio compared to monodomain samples. Only selected samples were aligned to form monodomains for investigation under SANS. The scattering trace for pure 5CB was used as a background.

5.4 Results

5.4.1 Polymer characteristics and phase behavior

A series of LC diblock copolymer samples were prepared in addition to an LC triblock copolymer (Table 5.1). The diblock copolymers were designed to investigate a series of block copolymers with varying PS block size, LC block size, and overall molecular weight. The diblock copolymers 590(40)AB, 530(60)AB, and 620(80)AB have similar LC block M_n but different PS block M_n . The diblocks 620(80)AB and 890(70)AB have similar PS block sizes with different LC block sizes. Finally, 450(120)AB and 840(190)AB have similar ratios of PS block M_n to LC block M_n with different overall M_n . These diblock copolymers can be compared to triblock copolymers 1320(60)ABA and

800(20)ABA which can form “bridges” where one polymer strand associates with two different micelles.

Table 5.1: Polymer characteristics

Polymer	PDI	LC Block Composition				
		LC Block M_n ($\frac{\text{kg}}{\text{mol}}$)	PS Block M_n ($\frac{\text{kg}}{\text{mol}}$)	1,2 Content (mol %)	1,4 Content (mol %)	Mesogen Content (mol %)
710LCP	1.08	713	0	8	3	89
500LCP	1.15	497	0	7	11	82
590(40)AB	1.37	592	40	21	1	78
530(60)AB	1.09	534	60	24	3	73
890(70)AB	1.11	886	70	18	12	70
620(80)AB	1.13	620	80	9	5	86
450(120)AB	1.65	445	120	31	1	68
840(190)AB	2.06	839	190	11	23	66
1320(60)ABA	1.40	1321	67,57	16	14	70
800(20)ABA	1.20	799	14,24	8	10	82

The phase behavior of PS [3] in 5CB and the present SGLCP [5] in 5CB has previously been studied. PS is insoluble in nematic 5CB, and the SGLCP was found to be soluble at all concentrations tested, up to concentrations of 20 wt %. Therefore, micelles formed by PS-SGLCP block copolymers in 5CB will consist of a PS core and an SGLCP corona.

All polymers were soluble in 5CB in both the nematic and isotropic phases at concentrations up to 10 wt %. Mixtures of 710LCP, 590(40)AB, 620(80)AB, 840(190)AB, and 800(20)ABA with 5CB had a biphasic region between the nematic and isotropic phases. The T_{NI} was taken to be the onset of this biphasic transition, observed under polarized optical microscopy. Pure 5CB has a T_{NI} of approximately 35.2 °C, and D5CB has a slightly lower T_{NI} of 33.5 °C.

Single phase mixtures of block copolymer in 5CB showed a homogenous nematic texture under the microscope. This agrees with previous studies [6], which found that LC diblock copolymers with large LC block fractions (greater than 90%) formed uniform nematic solutions, as observed under optical microscopy. In contrast, Finkelmann and coworkers observed that block copolymers with smaller LC block fractions can form micrometer-thick, phase-separated threads when mixed with a small molecule nematic LC [6].

5.4.2 Neutron scattering

SANS experiments give information about structure present on various length scales. Information at larger length scales is reflected at smaller scattering angles, and the characteristic length scale is inversely related to the scattering vector $q = (4\pi/\lambda) \sin(\theta/2)$. We performed SANS experiments with q ranging between 0.0067 \AA^{-1} and 1.0 \AA^{-1} . Scattering at low q ($< 0.03 \text{ \AA}^{-1}$) reveals information about micellar ordering and structure. The mid- q region of the scattering pattern ($0.03 \text{ \AA}^{-1} < q < 0.10 \text{ \AA}^{-1}$) reflects intrachain correlations, and the high q region gives information about the concentration of scattering centers in the sample and reflects incoherent background scattering.

Scattering experiments were performed on monodomain SGLCP homopolymer 710LCP in D5CB to investigate the conformation of the SGLCP in solution. The scattering pattern for SGLCP homopolymer 710LCP shows much stronger scattering in the direction perpendicular rather than parallel to the director (Fig. 5.1), indicating that the polymer backbone conformation is anisotropic and preferentially extended along the nematic director. The bow-tie shape observed in the scattering pattern has previously been observed in highly extended side-on side-group LC polymers [7, 8] and main-chain LC polymers [9] and suggests a highly extended polymer conformation. A Debye model fit gives an approximate anisotropy R_{\parallel}/R_{\perp} of 5 [5]. Neutron scattering patterns for shear-aligned triblock gels show that the anisotropy observed for SGLCP homopolymer in solution is also present in the physically associated polymer network (Fig. 5.2). The scattering patterns for the gels exhibit a smaller anisotropy compared to the SGLCP homopolymer. For both 710LCP and 1320(60)ABA, the scattering patterns are isotropic for temperatures higher than the T_{NI} .

SANS experiments on polydomain diblock and triblock polymers in D5CB reveal the micellar structure present (all SANS data is given at the end of the chapter in Section 5.6). For samples at a given concentration, the data converge onto a single curve in the mid- q region of the spectrum, overlapping with the SANS data for an SGLCP homopolymer of a similar concentration (Fig. 5.3). Therefore, the mid- q region is dominated by single chain contributions. Micellar structure is reflected at lower q , and, relative to homopolymers, diblock and triblock copolymers have significant low- q scattering in the nematic phase (Fig. 5.3). While block copolymer micelles in selective isotropic

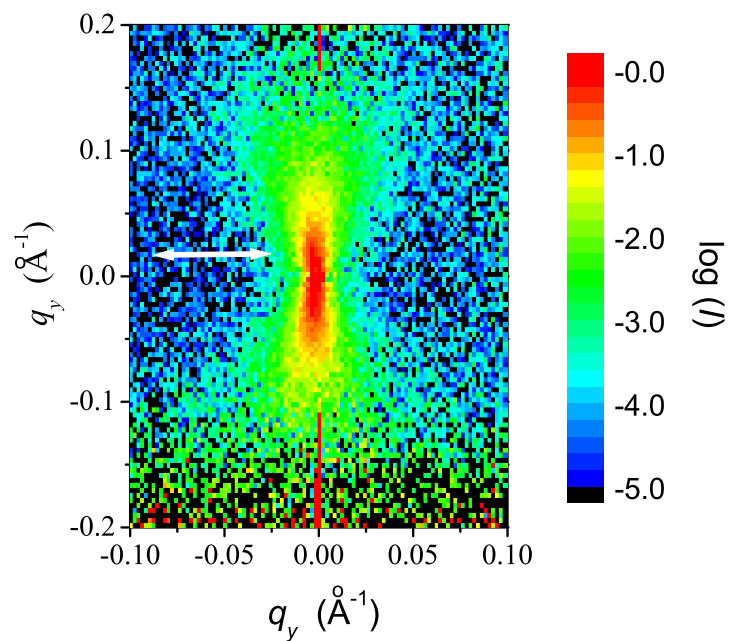


Figure 5.1: Neutron scattering pattern for a monodomain solution of 710LCP in perdeuterated 5CB. Uniform alignment was achieved by coating the cell surface with a rubbed polyimide layer. The double-headed arrow denotes the director, and q_x and q_y denote components of the scattering vector.

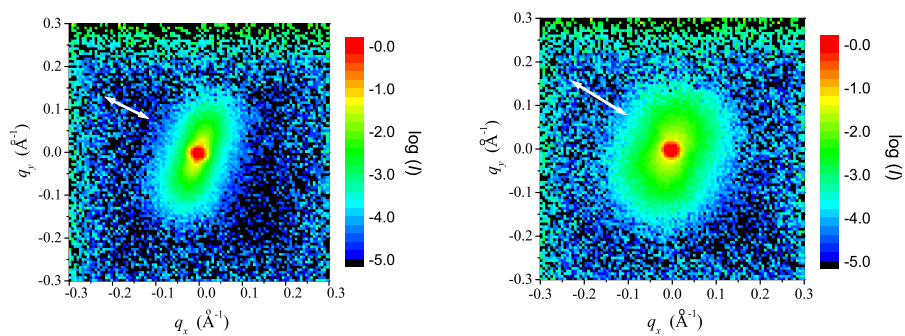


Figure 5.2: Neutron scattering pattern for shear-aligned 1320(60)ABA in D5CB at 5 wt % (left), and 10 wt % (right). The double-headed arrow denotes the director, and q_x and q_y denote components of the scattering vector. The samples were shear aligned by hand.

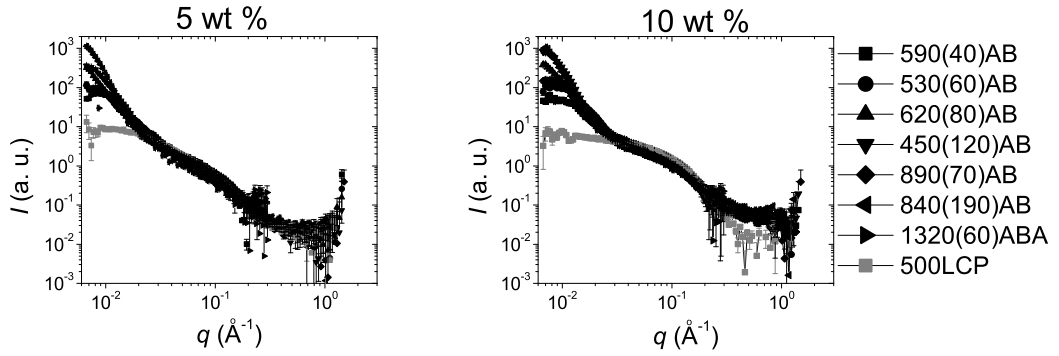


Figure 5.3: Neutron scattering pattern for LC polymers in D5CB. All data are for polydomain samples at 25 °C, with the exception of 890(70)AB and 1320(60)ABA. The scattering pattern for 890(70)AB was collected at 29 °C. 1320(60)ABA was aligned by shear, and the data shown were averaged over a 15° wedge region oriented along the direction parallel to the director.

solvents oftentimes assemble into hexagonally ordered phases [10, 11, 12, 13], the block copolymer micelles in the present system are disordered, as evidenced by the absence of Bragg lattice peaks.

In principle, we would like to fit the scattering patterns with an appropriate model that includes the form factor of the micelle along with a structure factor that accounts for micelle-micelle correlations [14, 15]. A proper fit could provide quantitative data about the size of the micelle core, the micelle corona, and the intermicellar distance [12, 16]. However, several difficulties impeded useful fitting of the data. The solvent is not matched to either block of the copolymer samples, and therefore the form factor must account for scattering from both the micellar cores and the corona. The cores may be highly swollen with solvent, and the aggregation number of the micelles is unknown. Therefore, fitting requires a large number of parameters that have not been independently measured. We therefore chose to rely on the qualitative features of the neutron scattering patterns to gain insight into the block copolymer structure and, in particular, its temperature dependence.

Diblock and triblock gels show one or more peaks in the scattering pattern at low q (Section 5.6). Most samples have a peak near $q = 0.008 \text{ \AA}^{-1}$, and data for 530(60)AB and 620(80)AB show a second peak near $q = 0.02 \text{ \AA}^{-1}$ (Figs. 5.5 and 5.7). The position of the first peak changes with temperature and concentration, and it depends on the polystyrene block length (Table 5.2). The position of

Table 5.2: Peak positions in 10^{-3} \AA^{-1} for block copolymer-D5CB mixtures at 25 °C, $T_{NI} - 2 \text{ °C}$, and $T_{NI} + 2 \text{ °C}$. The lowest q probed is $6.7 \cdot 10^{-3} \text{ \AA}^{-1}$. “NP” means “no peak”.

Polymer	25 °C		$T_{NI} - 2 \text{ °C}$		$T_{NI} + 2 \text{ °C}$	
	5 wt %	10 wt %	5 wt %	10 wt %	5 wt %	10 wt %
560(40)AB	9.8	9.8	10.8	10.8	NP	NP
540(60)AB	8.1	8.1	8.1	7.7	NP	NP
850(70)AB	8.1	8.9	N/A	N/A	N/A	N/A
600(80)AB	≤ 6.7	≤ 6.7	≤ 6.7	≤ 6.7	NP	NP
410(120)AB	≤ 6.7	≤ 6.7	7.0	7.4	7.0	7.4
910(190)AB	7.0	7.0	7.0	7.0	7.0	7.0
1340(60)ABA	≤ 8.7	≤ 8.7	N/A	N/A	NP	NP

the peak is qualitatively correlated with the size of the micelles. In most mixtures, the peak shifts to higher q with increasing polymer composition and temperature. For example, at 25 °C, three diblock samples have peaks below 0.067 \AA^{-1} , but above the T_{NI} two of these peaks shift to higher q and only the 600(80) gels retain peaks below 0.067 \AA^{-1} . The PS block length also affects the peak position, as can be seen by comparing the diblock series 564(40)AB, 540(60)AB, 600(80)AB, and 410(120)AB (see the data for $T_{NI} + 2$). The peak shifts to lower q with increasing PS block length. These results show that smaller micelles are formed at higher polymer concentrations, higher temperatures, and with copolymers with smaller PS block lengths.

Increasing the temperature across the T_{NI} significantly diminishes the low- q scattering for most but not all mixtures (Section 5.6). The loss of low- q scattering is associated with the loss of microphase separated structure, and the temperature above which the copolymers exist as free chains in solution is known as the microphase separation temperature T_{MST} . We use the expression microphase separation temperature to distinguish the present samples from block copolymer micelles which are ordered on a periodic lattice and show order-disorder transitions [17], although the terms are oftentimes used interchangeably [18]. Diblock and triblock copolymers with PS block smaller than 80 kg/mol show a T_{MST} coincident with the T_{NI} of the gel (Figs. 5.4, 5.5, 5.6, and 5.10). This is clearly shown by a dramatic drop in low- q intensity and loss of features in the data at low q . The diffuse excess scattering observed for 530(60)AB (Fig. 5.5) is likely due to compositional fluctuations

in the vicinity of the T_{MST} [17]. By contrast, diblock copolymers with larger PS blocks show low- q scattering above the T_{NI} for some concentrations. In the case of 530(60)AB, a 5 wt % mixture has a T_{MST} coincident with the T_{NI} , but a 10 wt % mixture shows significant low- q scattering with discernable features up to 40 °C (Fig. 5.7). 450(120)AB mixtures with 5CB show micellar structure above the T_{NI} for both 5 wt % and 10 wt % mixtures. The T_{MST} is approximately 50 °C for 10 wt % 450(120)AB (Fig. 5.8). In the case of 840(190)AB, 5 and 10 wt% gels show significant low- q scattering at all temperatures tested, up to 60 °C (Fig. 5.9).

Increasing the temperature within the nematic phase also results in decreased scattering at low q . A decreased volume fraction of micelles due to an increasing number of free chains is unlikely given the low solubility of PS in nematic 5CB [3]. If the concentration of associated chains is independent of temperature in the nematic phase and micelles are assumed to be non-overlapping particles, then decreased scattering at low q is correlated with a smaller aggregation number [19].

5.4.3 Rheometry

Dynamic mechanical rheological measurements at low strains give information about the equilibrium mechanical properties of the diblock and triblock copolymer mixtures with 5CB. The data from dynamic rheological measurements for all the diblock and triblock copolymer mixtures in 5CB is given in Section 5.7. The various samples with different PS and SGLCP block lengths and polymer architecture (diblock vs. triblock) share many characteristics in their rheological behavior. All the systems show solid-like behavior at sufficiently high polymer concentrations, with $G' \gg G''$ and a plateau modulus over a wide range of frequencies. These properties are characteristic of crosslinked rubbers [20]. For the purposes of this study, the term “gel” will refer to a mixture that exhibits solid-like behavior over a wide range of frequencies [21]. The mixtures that do not show solid-like behavior in the nematic phase (e.g., 5 wt % 530(60)AB at 25 °C, Fig. 5.13), do show viscoelastic behavior in the nematic phase – their rheological behavior is not like that of an elastic solid ($G' \gg G''$, and G' frequency independent) nor a like that of a liquid ($G'' \gg G'$, $G' \sim \omega^2$, $G'' \sim \omega$).

Both diblock and triblock LC copolymers can form gels in 5CB, as evidenced by the rheological

behavior of 5 wt % 850(70)AB (Fig. 5.15) and 5 wt % 1340(6)ABA (Fig. 5.23). Bridging between micelles, where one polymer strand has its end associated in two different micelle cores, is only possible in triblock copolymer mixtures. The fact that diblock LC copolymers can form gels indicates that micellar repulsion plays an important role in gelation. These diblock and triblock gels share characteristics with the “soft” gel phases [11, 13, 22], which are disordered and have a modulus significantly lower than that for ordered micellar phases, typically 10^4 Pa [13].

In all mixtures studied, significant changes to the rheological behavior were observed with temperature, in particular near the T_{NI} (e.g., Figs. 5.24 and 5.22). Many mixtures transition from viscoelastic behavior below the T_{NI} to terminal behavior ($G' \ll G''$, $G'' \sim \omega$) above the T_{NI} (e.g., Fig. 5.15). All the mixtures exhibited liquid-like behavior at sufficiently high temperatures, but recovered their viscoelastic behavior on cooling (e.g., Figs. 5.24 and 5.22). In addition, increasing the temperature within the nematic phase results in a decreased storage modulus for all diblock and triblock mixtures.

The rheological behavior of the SGLCP block copolymer – 5CB mixtures depends on the PS and SGLCP block lengths. Diblock copolymers with larger PS blocks have higher storage moduli at a particular concentration, as shown in the series 590(40)AB, 530(60)AB, and 620(80)AB at a concentration of 10 wt % (Table 5.3). Furthermore, diblock copolymers with larger PS block lengths more readily show gel-like behavior. For example, the dynamic rheometry measurements show that 5 wt % 620(80)AB is a gel (Fig. 5.17), while 5 wt % 590(40)AB and 530(60)AB are viscoelastic liquids (Figs. 5.11 and 5.13). Diblock copolymers with longer SGLCP blocks also have a higher storage modulus, as can be seen by comparing 890(70)AB to 530(60)AB (Table 5.3).

The sol-gel transition temperature, which marks the transition from solid-like behavior to liquid-like behavior, also depends on the PS block length of the copolymer in the mixture. The sol-gel transition is taken to be the temperature above which the loss modulus exceeds the storage modulus ($G'' > G'$) at a frequency of 1 rad/s. Almost all the samples studied have a sol-gel transition coincident with the T_{NI} (Table 5.4). Two notable exceptions are gels formed by the copolymers with the largest PS blocks, 840(190)AB and 450(120)AB. In the case of 5 wt % 840(190)AB, the

Table 5.3: Gel storage modulus (Pa) at 20 °C and 1 rad/s

Polymer	5 wt %	10 wt %
590(40)AB	4.52	53.3
530(60)AB	2.93	99.4
890(70)AB	28.8	202
620(80)AB	29.1	201
450(120)AB	14.9	142
840(190)AB	48.5	100
1320(60)ABA	68.6	192
800(20)ABA	70.3	196

sol-gel transition occurs well above the T_{NI} of the gel, at approximately 42 °C (Fig. 5.22). Also, 10 wt % 450(120)AB exhibits a significant range of temperatures above the T_{NI} , up to 40 °C, where it exhibits viscoelastic behavior with $G' \sim G''$ (Figs. 5.35 and 5.36).

This temperature-dependent and frequency-dependent behavior suggest that the PS aggregates are not glassy (even though T_g for PS is ~ 105 °C). Polymers linked together with glassy crosslinks exhibit solid-like behavior at all frequencies [23]. For the present samples, we observe liquid like behavior at low frequencies, especially near the T_{NI} . For example, 5 wt % 1320(60)ABA shows liquid-like behavior at 34 °C for frequencies lower than 0.1 rad/s (Fig. 5.23). We conclude that the PS endblocks are swollen with LC solvent and that PS endblocks can disengage from the physical crosslinks on finite time scales. This is consistent with the “slow” dynamic relaxation processes observed in dynamic light scattering studies (Chapter 4).

A comparison between the rheological behavior of triblock and diblock samples shows that bridging does take place in triblock gels and increases the modulus relative to diblock gels. Diblock 530(60)AB has a matching PS endblock and the same mass ratio of PS to SGLCP as that of triblock 1320(60)ABA. Triblock 1320(60)ABA forms a gel at 5 wt % (Fig. 5.23), but a 5 wt % mixture of 530(60)AB does not (Fig. 5.13). A comparison of 590(40)AB and 800(20)ABA, which has a shorter PS block, provides further evidence of bridging. While 5 wt % 800(20)ABA exhibits a plateau modulus at low temperatures (Fig. 5.25), 5 wt % 590(40)AB does not (Fig. 5.11).

We can gain insight into the relationship between micelle formation and the gels' rheological

Table 5.4: The reduced temperature $T - T_{NI}$ for the sol-gel transition measured by rheology and the T_{MST} measured by SANS. The rheological measurement is the temperature (while heating) at which the storage modulus drops below the loss modulus, and the SANS measurement is the lowest temperature at which the low- q scattered intensity is significantly diminished (overlapping or nearly overlapping with the SANS data for 710LCP) and lacks features characteristic of micellar structure.

Polymer	Rheology ($^{\circ}\text{C}$)		SANS ($^{\circ}\text{C}$)	
	5 wt %	10 wt %	5 wt %	10 wt %
590(40)AB	no gel	-1.0	3.0	2.0
530(60)AB	no gel	-0.5	7.5	6.5
890(70)AB	0.0	0.0	4.5	4.5
620(80)AB	1.5	1.5	7.5	3.5
450(120)AB	-1.0	2.5	>17.0	16.5
840(190)AB	6.0	17	>27.5	>27.5
1320(60)ABA	0.0	0.0	6.5	6.5

properties by comparing the temperatures at which micellar structure vanishes in the SANS experiments to the sol-gel transition measured by rheology (Table 5.4). The neutron scattering experiments are performed at much larger temperature intervals, and therefore they necessarily have a greater uncertainty in temperature. Nevertheless, the comparison shows an interesting correlation between micelle formation and rheology. First, the data suggest that micelles can persist well above the sol-gel transition measured by rheology. In the most extreme case, 910(190)AB gels display a sol-gel transition at 45 $^{\circ}\text{C}$, but micelles persist up to at least 60 $^{\circ}\text{C}$. The data also show that the location of the sol-gel transition is correlated with micelle formation. Diblocks that gel in 5CB above the T_{NI} (600(80)AB, 410(120)AB, and 910(190)AB) also show low- q scattering far into the isotropic phase (Table 5.4).

5.5 Discussion

LC gels formed by diblock and triblock LC copolymers represent a novel example of block copolymer self-assembly for two distinct reasons. First, the gel structure inherits the anisotropy of the host solvent. Micelles are anisotropic, as is the interconnected micellar network present in triblock gels. This anisotropy in the gel structure has significance for texture transitions and dynamic properties

of the gels, as discussed in Chapters 3 and 4. A second reason arises from the existence of a nematic-to-isotropic phase transition of the solvent. The solvent quality for the isotropic PS blocks changes drastically across the T_{NI} , resulting in significant structural changes in a small temperature window. This can result in useful properties, such as a thermoreversible gelation, and is also interesting for the potentially novel phase transitions that may arise [24].

The SANS and rheometry results establish several trends for the diblock and triblock copolymer micelle structure with temperature, concentration, and block sizes. SANS reveals smaller micelles at higher polymer concentrations and higher temperatures, and the aggregation number decreases with temperature in the nematic phase. SANS also reveals that a larger PS block length is correlated with an increase in the T_{MST} . Rheometry reveals a decreased storage modulus with temperature in the nematic phase and an increased sol-gel transition temperature for copolymers with larger PS blocks.

The neutron scattering and rheometry studies establish a relationship between micelle formation and the mechanical properties of the gel. Micelle formation drives gel formation through intermicellar interactions, namely micelle-micelle repulsion and bridging between micelles. These interactions are temperature dependent. Increasing the temperature within the nematic phase decreases the size of the micelles, which corresponds with a decreasing storage modulus. Heating the sample above the T_{NI} oftentimes results in loss of physical associations, resulting in a drop in the modulus and a transition to a sol state. In some cases, the T_{MST} is significantly higher than the sol-gel transition temperature (see 10 wt % 620(80)AB, Figs. 5.7 and 5.33). In this case, micelles may exist in a “gas-like” state of non-interacting micelles above the sol-gel transition temperature [11]. The positional correlations of the micelles has a finite lifetime even in triblock gels, demonstrating that the PS endblocks are not glassy but plasticized by LS solvent. Furthermore, the strength of self-assembly that drives gel formation can be controlled by increasing the size of the PS blocks, which increases the driving force for self assembly and results in stiffer gels, higher sol-gel transition temperatures, and a higher T_{MST} .

Based on the relative sizes of the PS and SGLCP blocks of the copolymers, we expect the micelles

to have a “hairy” structure, with an extended corona and a much smaller core [25]. Scaling arguments by Halperin et al. for “hairy” micelles predict that the aggregation number is strongly dependent on the PS-core block size [25]. The SANS data show an increasing micelle size with increasing PS block size (Table 5.2), consistent with this prediction. The physical picture of “hairy” micelles suggests that coronal repulsions may play an equal or dominant role to bridging in determining intermicellar interaction, which can explain the comparable dynamic rheological behavior observed for 1320(60)ABA (Fig. 5.23) and 870(70)AB (Fig. 5.15). Also, this may explain the lack of ordering observed for the diblock mixtures, which in a separate study were investigated to concentrations as high as 20 wt % [24]. “Hairy” micelles are expected to have a softer intermicellar potential, reducing the tendency for long-range lattice ordering, although few experimental studies exist to corroborate this [13, 22].

In summary, SANS experiments and rheometry found that the micellar structure of LC block copolymer gels changes significantly across the T_{NI} . The loss of orientational order of the LC solvent is associated with a decreased selectivity for the isotropic PS block and an associated loss of micellar structure in many cases. The size of the PS block is an important variable determining the driving force for self-assembly, with larger PS blocks associated with gelation even above the T_{NI} . No long-range lattice order was exhibited by the copolymer micellar gels, and this may be related to the “hairy” structure of the block copolymer micelles.

5.6 SANS of diblock and triblock gels

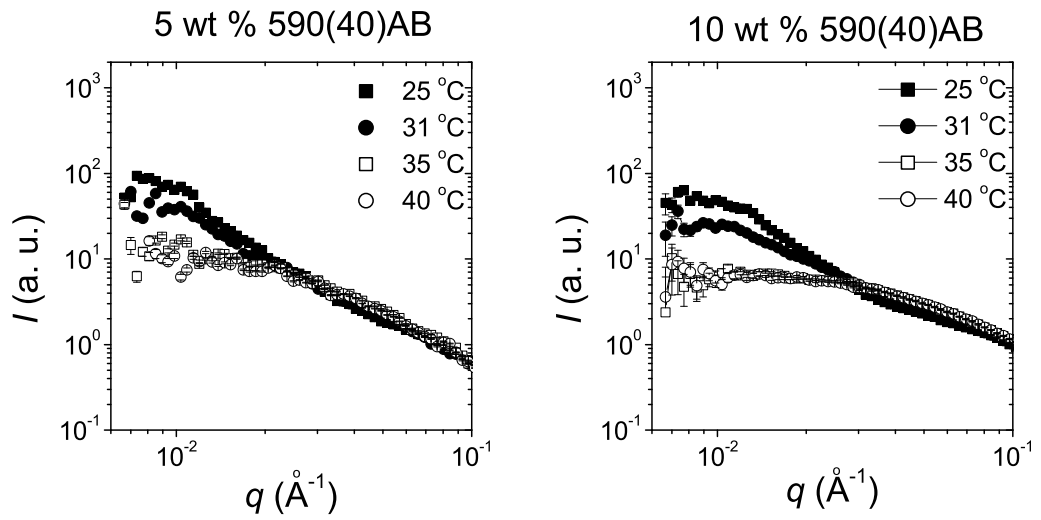


Figure 5.4: Azimuthally averaged SANS pattern for 5 and 10 wt % 590(40)AB in perdeuterated 5CB. The 5 wt % mixture is single-phase nematic for all $T \leq 32.1$ °C and single-phase isotropic for $T \geq 34.0$ °C. The 10 wt % mixture is single-phase nematic for all $T \leq 33.0$ °C and single-phase isotropic for $T \geq 36.0$ °C.

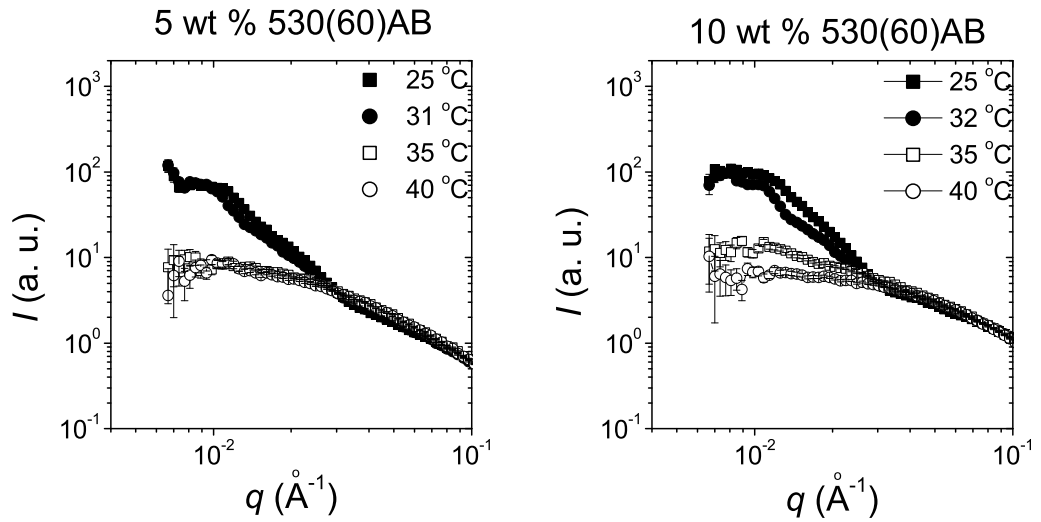


Figure 5.5: Azimuthally averaged SANS pattern for 5 and 10 wt % 530(60)AB in perdeuterated 5CB. The 5 wt % mixture is single-phase nematic for all $T \leq 32.5$ °C and single-phase isotropic for $T \geq 34.0$ °C. The 10 wt % mixture is single-phase nematic for all $T \leq 33.5$ °C and single-phase isotropic for $T \geq 34.5$ °C.

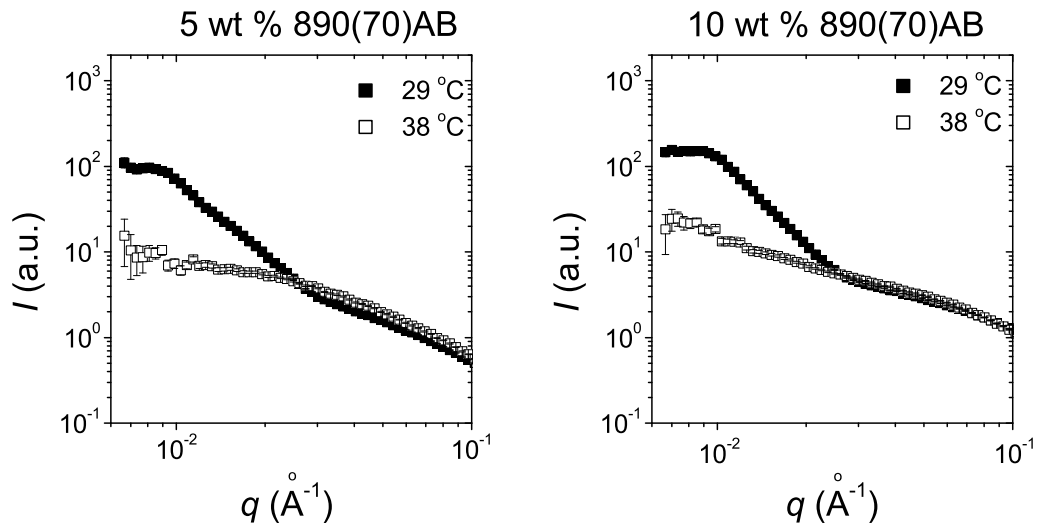


Figure 5.6: Azimuthally averaged SANS pattern for 5 and 10 wt % 890(70)AB in perdeuterated 5CB. The mixtures are single-phase nematic for all $T \leq 33.5$ °C and single-phase isotropic for $T > 33.5$ °C.

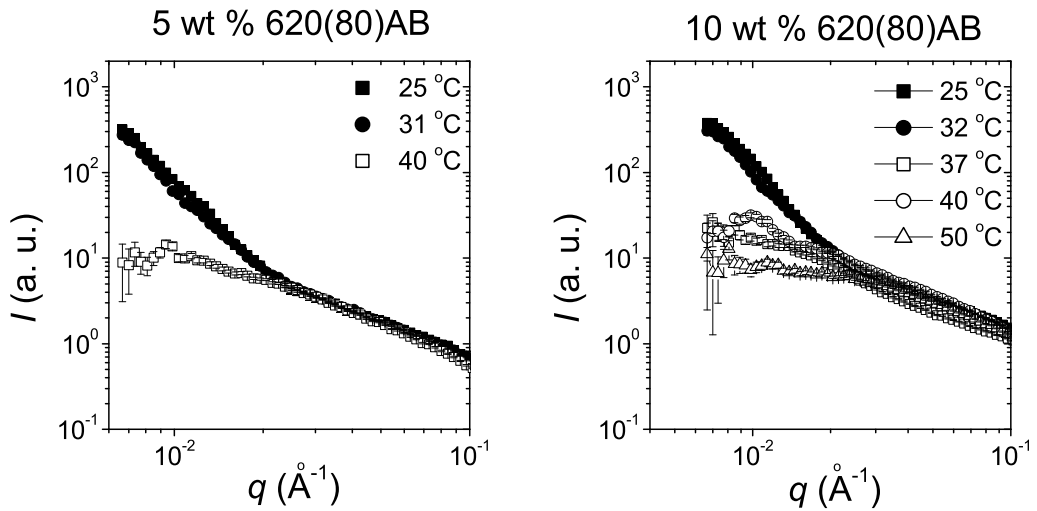


Figure 5.7: Azimuthally averaged SANS pattern for 5 and 10 wt % 620(80)AB in perdeuterated 5CB. The 5 wt % mixture is single-phase nematic for all $T \leq 32.5$ °C and single-phase isotropic for $T \geq 39.0$ °C. The 10 wt % mixture is single-phase nematic for all $T \leq 33.5$ °C and single-phase isotropic for $T \geq 38.5$ °C.

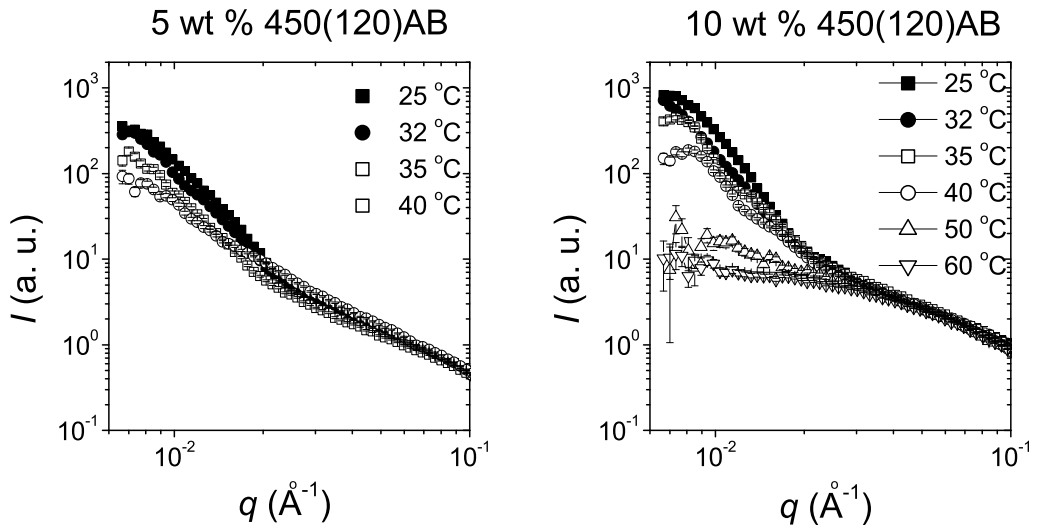


Figure 5.8: Azimuthally averaged SANS pattern for 5 and 10 wt % 450(120)AB in perdeuterated 5CB. The 5 wt % mixture is single-phase nematic for all $T \leq 33.0$ °C and single-phase isotropic for $T \geq 34.0$ °C. The 10 wt % mixture is single-phase nematic for all $T \leq 33.5$ °C and single-phase isotropic for $T \geq 34.0$ °C.

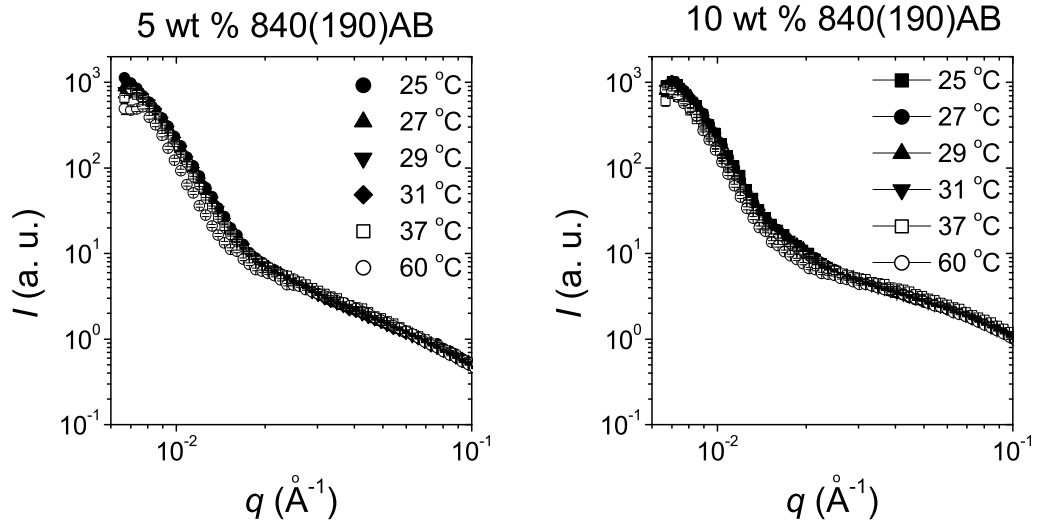


Figure 5.9: Azimuthally averaged SANS pattern for 5 and 10 wt % 840(190)AB in perdeuterated 5CB. The 5 wt % mixture is single-phase nematic for all $T \leq 32.9$ °C and single-phase isotropic for $T > 32.9$ °C. The 10 wt % mixture is single-phase nematic for all $T \leq 31.5$ °C and single-phase isotropic for $T \geq 34.7$ °C.

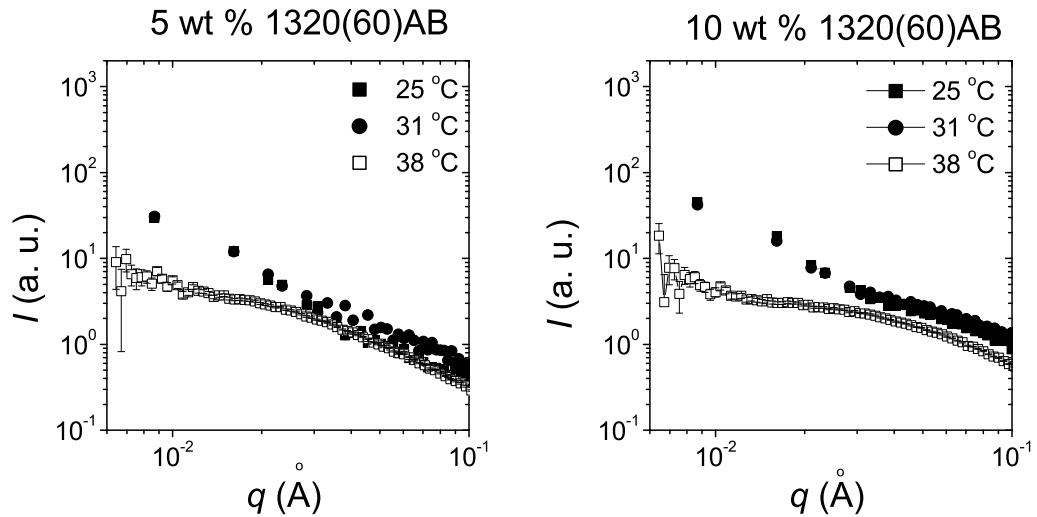


Figure 5.10: SANS pattern for 5 and 10 wt % 1320(60)ABA in D5CB. The data shown is averaged over a 15° wedge oriented along the nematic director. Both the 5 and 10 wt % mixtures are single-phase nematic for all $T \leq 33.5$ °C and single-phase isotropic for $T > 33.5$ °C.

5.7 Rheometry of diblock and triblock mixtures

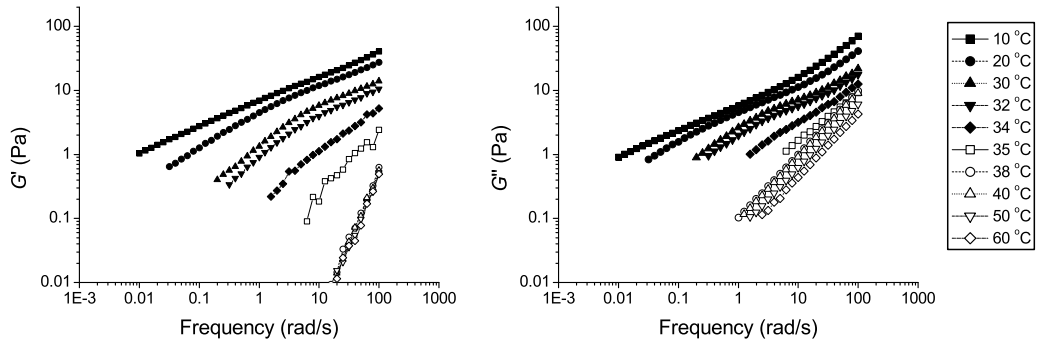


Figure 5.11: Dynamic storage modulus (G') and loss modulus (G'') of 5 wt % 590(40) AB diblock in 5CB. The mixture is single-phase nematic for all $T \leq 35.5$ °C (closed symbols) and single-phase isotropic for $T \geq 37.5$ °C (open symbols).

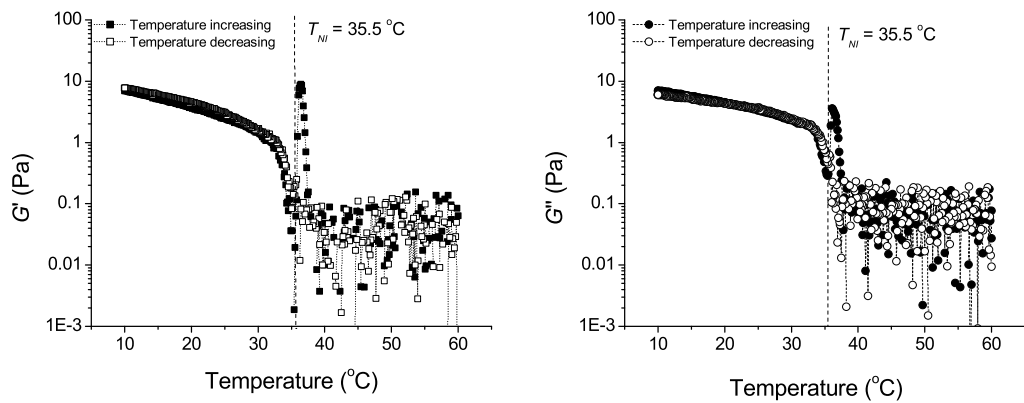


Figure 5.12: Dynamic storage modulus (G') and loss modulus (G'') of 5 wt % 590(40) AB diblock in 5CB while heating (closed symbols) and cooling (open symbols) at 0.5 °C/min

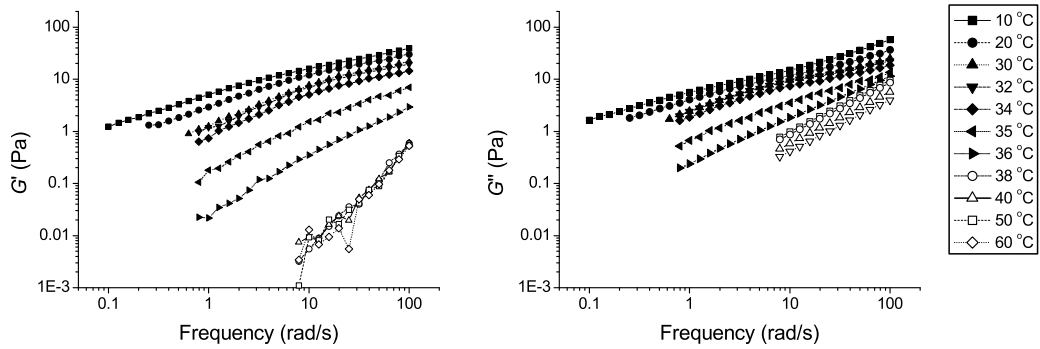


Figure 5.13: Dynamic storage modulus (G') and loss modulus (G'') of 5 wt % 530(60) AB diblock in 5CB. The mixture is single-phase nematic for all $T \leq 36.0$ °C (closed symbols) and single-phase isotropic for $T > 36.0$ °C (open symbols).

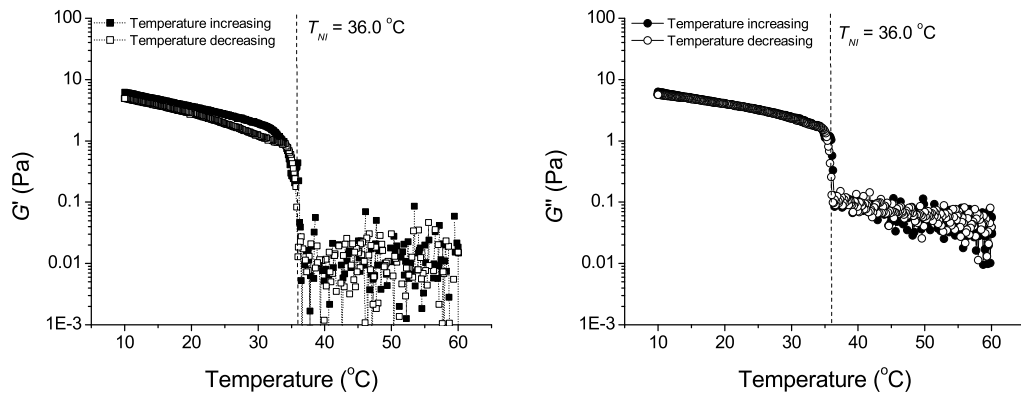


Figure 5.14: Dynamic storage modulus (G') and loss modulus (G'') of 5 wt % 530(60) AB diblock in 5CB while heating (closed symbols) and cooling (open symbols) at 0.5 °C/min

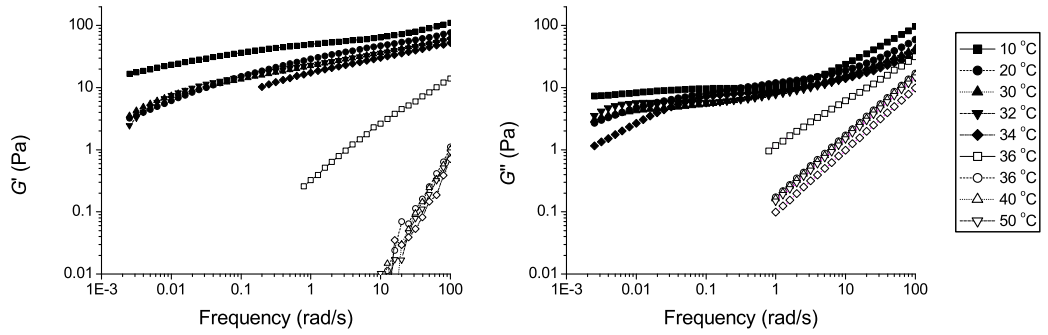


Figure 5.15: Dynamic storage modulus (G') and loss modulus (G'') of 5 wt % 890(70) AB diblock in 5CB. The mixture is single-phase nematic for all $T \leq 35.9$ °C (closed symbols) and single-phase isotropic for $T > 35.9$ °C (open symbols).

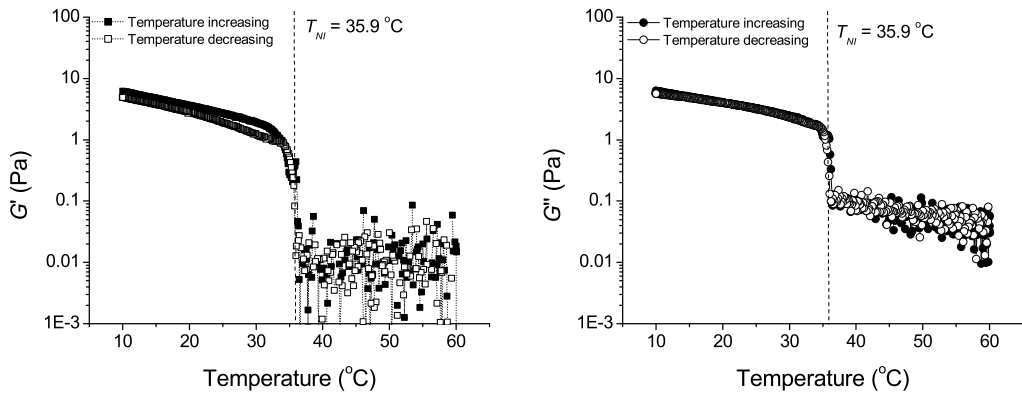


Figure 5.16: Dynamic storage modulus (G') and loss modulus (G'') of 5 wt % 890(70) AB diblock in 5CB while heating (closed symbols) and cooling (open symbols) at 0.5 °C/min

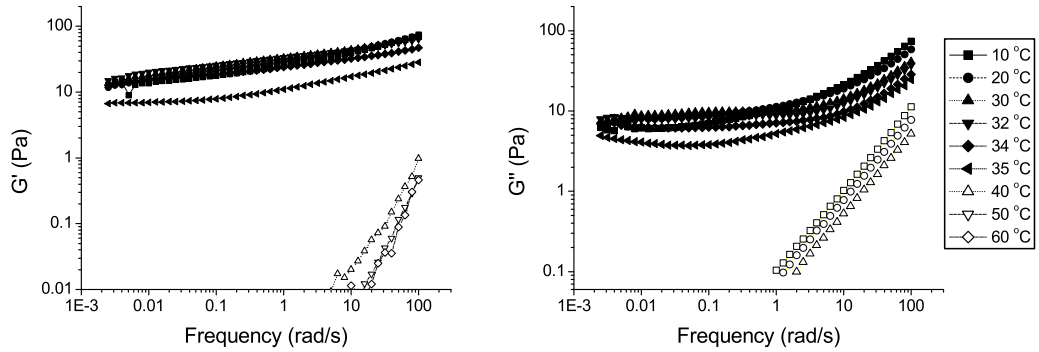


Figure 5.17: Dynamic storage modulus (G') and loss modulus (G'') of 5 wt % 620(80)AB diblock in 5CB. The mixture is single-phase nematic for all $T \leq 35.5$ °C (closed symbols) and single-phase isotropic for $T \geq 40.0$ °C (open symbols).

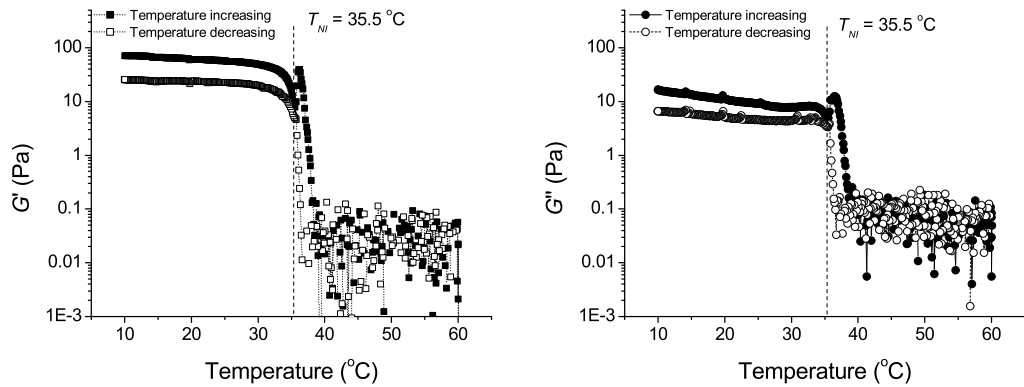


Figure 5.18: Dynamic storage modulus (G') and loss modulus (G'') of 5 wt % 620(80) AB diblock in 5CB while heating (closed symbols) and cooling (open symbols) at 0.5 °C/min

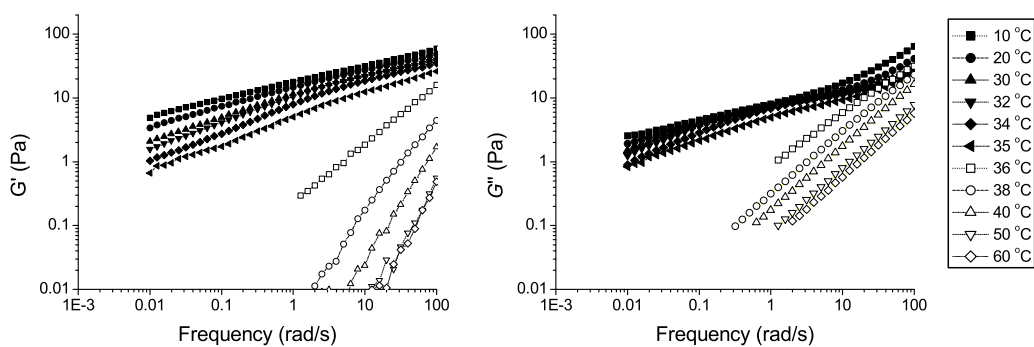


Figure 5.19: Dynamic storage modulus (G') and loss modulus (G'') of 5 wt % 450(120) AB diblock in 5CB. The mixture is single-phase nematic for all $T \leq 35.8$ °C (closed symbols) and single-phase isotropic for $T > 35.8$ °C (open symbols).

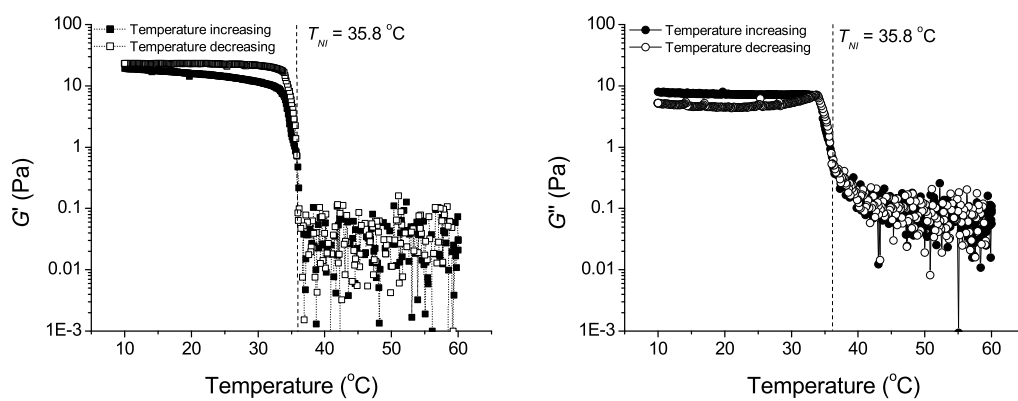


Figure 5.20: Dynamic storage modulus (G') and loss modulus (G'') of 5 wt % 450(120) AB diblock in 5CB while heating (closed symbols) and cooling (open symbols) at 0.5 °C/min

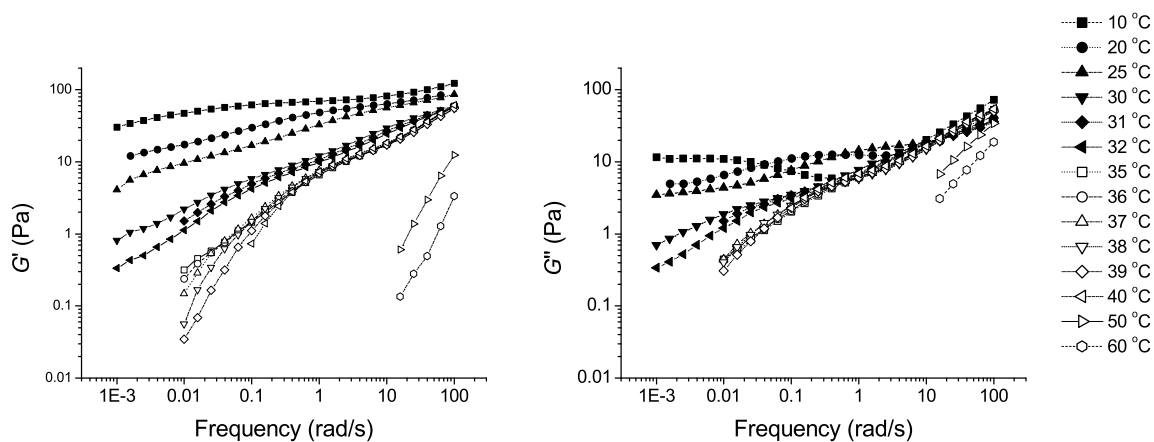


Figure 5.21: Dynamic storage modulus (G') and loss modulus (G'') of 5 wt % 840(190) AB diblock in 5CB. The mixture is single-phase nematic for all $T \leq 32.0$ °C (closed symbols) and single-phase isotropic for $T \geq 35.0$ °C (open symbols).

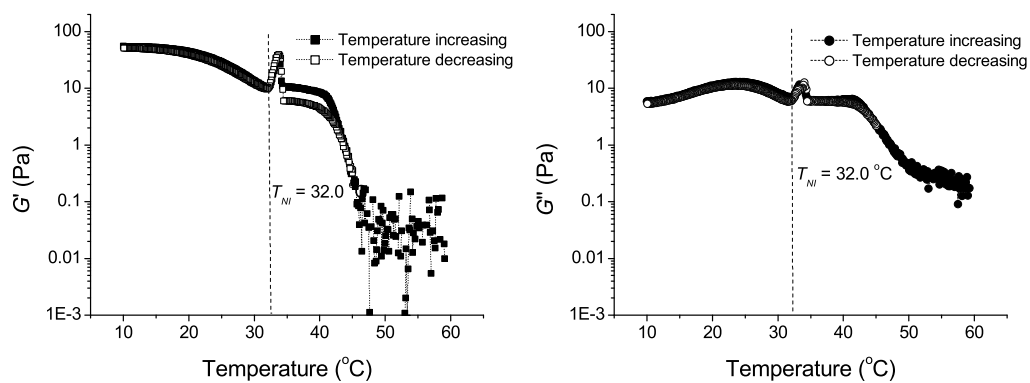


Figure 5.22: Dynamic storage modulus (G') and loss modulus (G'') of 5 wt % 840(190) AB diblock in 5CB while heating (closed symbols) and cooling (open symbols) at 0.5 °C/min

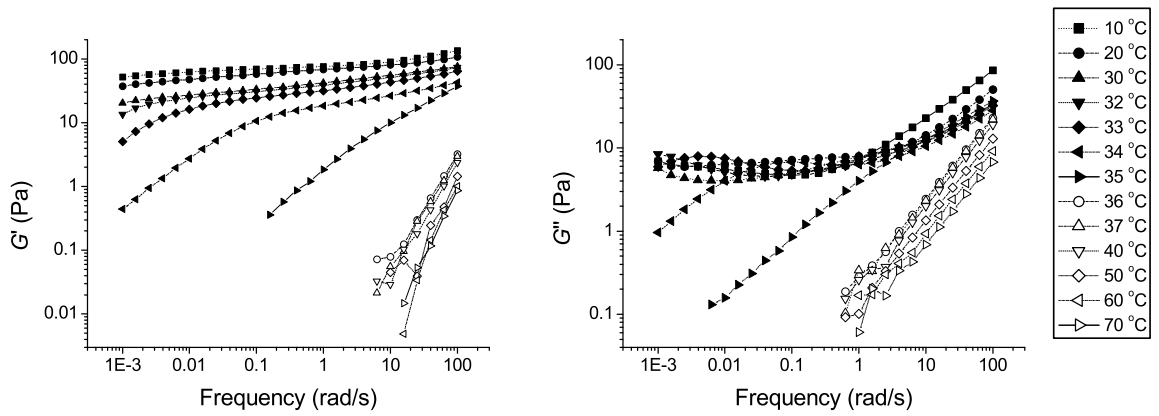


Figure 5.23: Dynamic storage modulus (G') and loss modulus (G'') of 5 wt % 1320(60) ABA in 5CB. The mixture is single-phase nematic for all $T \leq 35.2$ °C (closed symbols) and single-phase isotropic for $T > 35.2$ °C (open symbols).

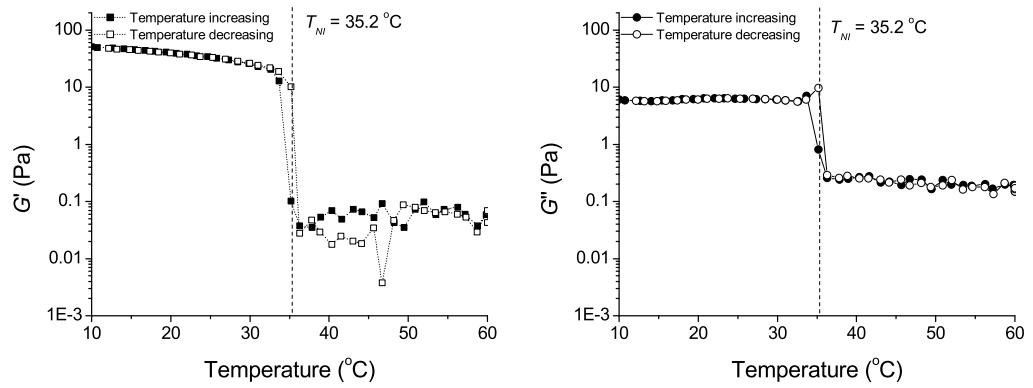


Figure 5.24: Dynamic storage modulus (G') and loss modulus (G'') of 5 wt % 1320(60) ABA triblock in 5CB while heating (closed symbols) and cooling (open symbols) at 5.0 °C/min

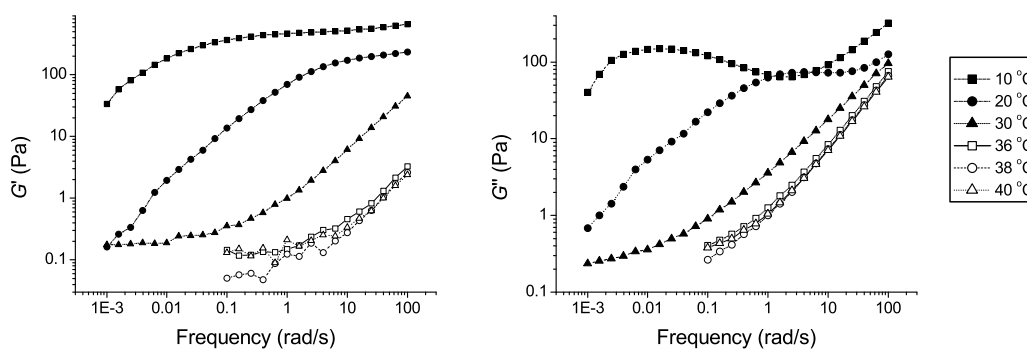


Figure 5.25: Dynamic storage modulus (G') and loss modulus (G'') of 5 wt % 800(20)ABA in 5CB. The mixture is single-phase nematic for all $T \leq 31.7$ °C (closed symbols) and single-phase isotropic for $T \geq 34.5$ °C (open symbols).

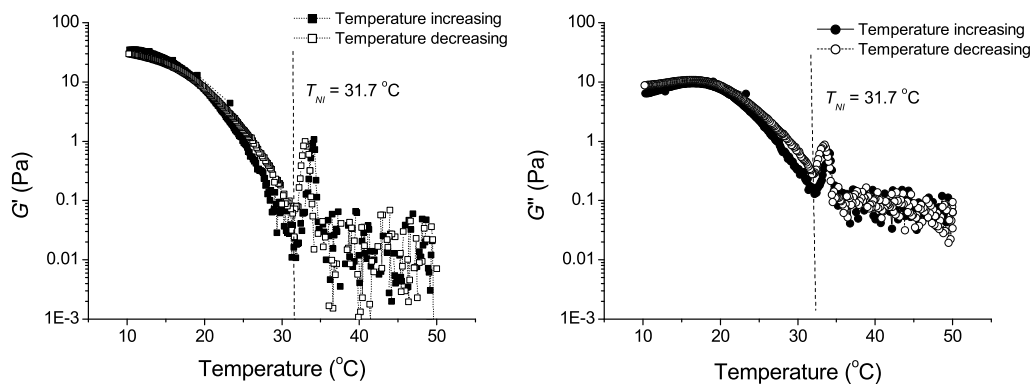


Figure 5.26: Dynamic storage modulus (G') and loss modulus (G'') of 5 wt % 800(20)ABA in 5CB while heating (closed symbols) and cooling (open symbols) at 0.5 °C/min

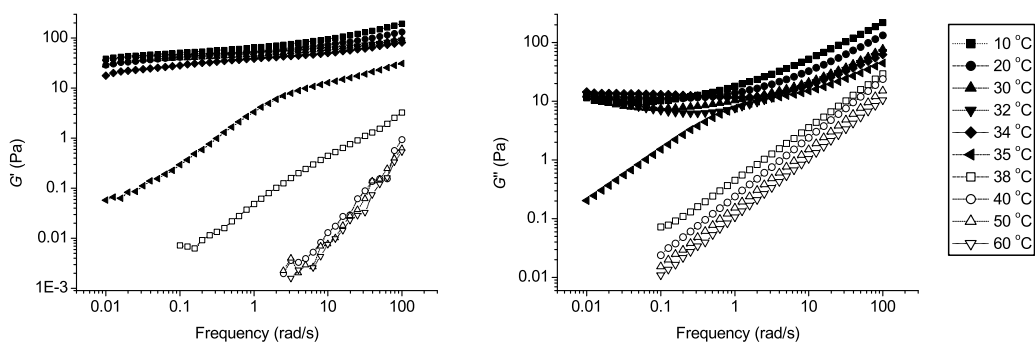


Figure 5.27: Dynamic storage modulus (G') and loss modulus (G'') of 10 wt % 590(40) AB diblock in 5CB. The mixture is single-phase nematic for all $T \leq 35.5$ °C (closed symbols) and single-phase isotropic for $T \geq 37.5$ °C (open symbols).

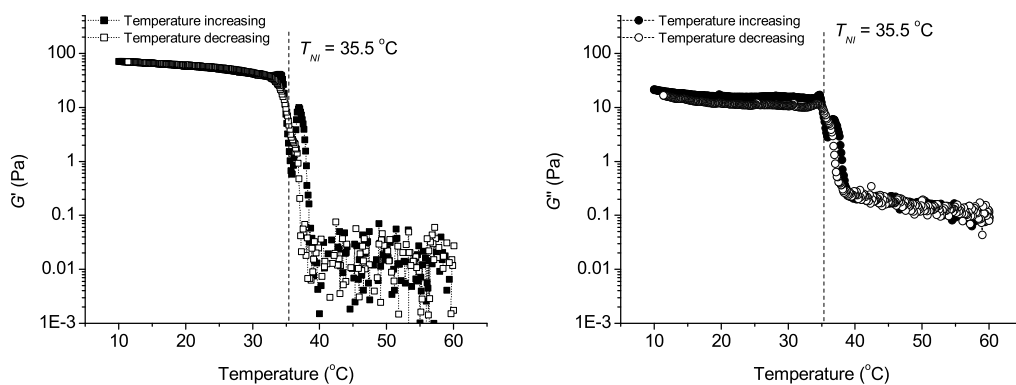


Figure 5.28: Dynamic storage modulus (G') and loss modulus (G'') of 10 wt % 590(40) AB diblock in 5CB while heating (closed symbols) and cooling (open symbols) at 0.5 °C/min

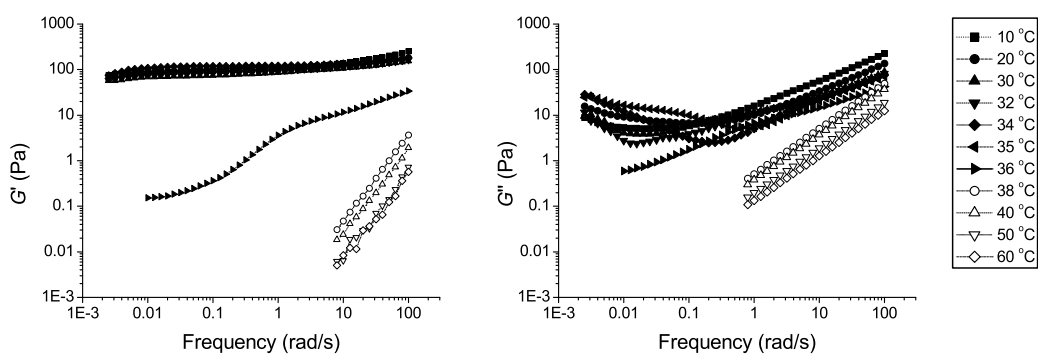


Figure 5.29: Dynamic storage modulus (G') and loss modulus (G'') of 10 wt % 530(60) AB diblock in 5CB. The mixture is single-phase nematic for all $T \leq 36.2$ °C (closed symbols) and single-phase isotropic for $T > 36.2$ °C (open symbols).

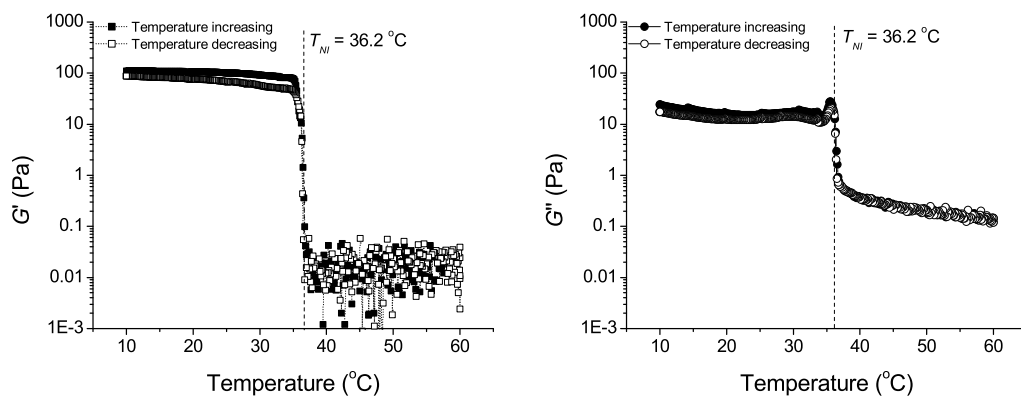


Figure 5.30: Dynamic storage modulus (G') and loss modulus (G'') of 10 wt % 530(60) AB diblock in 5CB while heating (closed symbols) and cooling (open symbols) at 0.5 °C/min

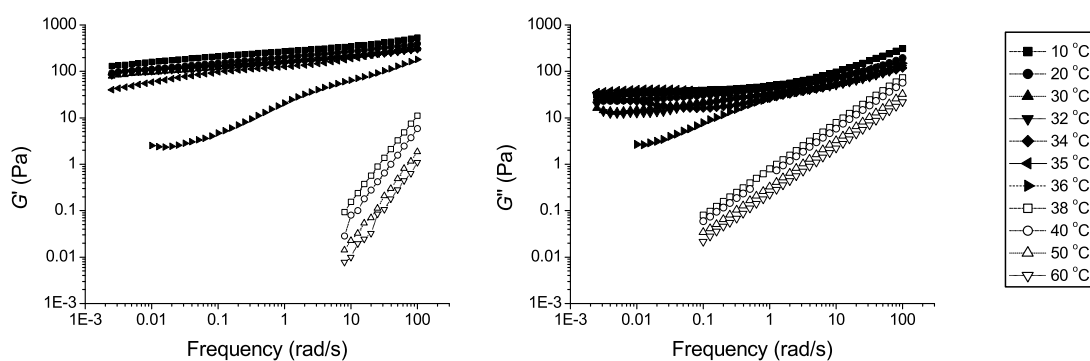


Figure 5.31: Dynamic storage modulus (G') and loss modulus (G'') of 10 wt % 890(70) AB diblock in 5CB. The mixture is single-phase nematic for all $T \leq 36.1$ °C (closed symbols) and single-phase isotropic for $T > 36.1$ °C (open symbols).

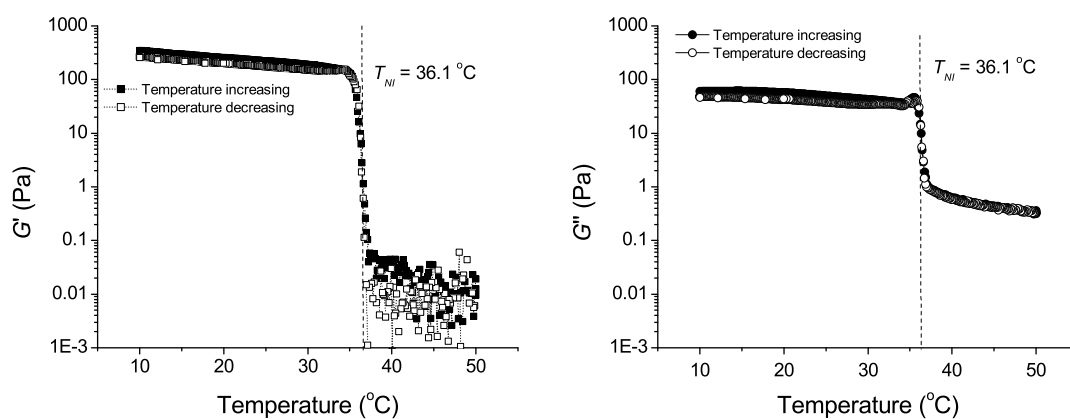


Figure 5.32: Dynamic storage modulus (G') and loss modulus (G'') of 10 wt % 890(70) AB diblock in 5CB while heating (closed symbols) and cooling (open symbols) at 0.5 °C/min

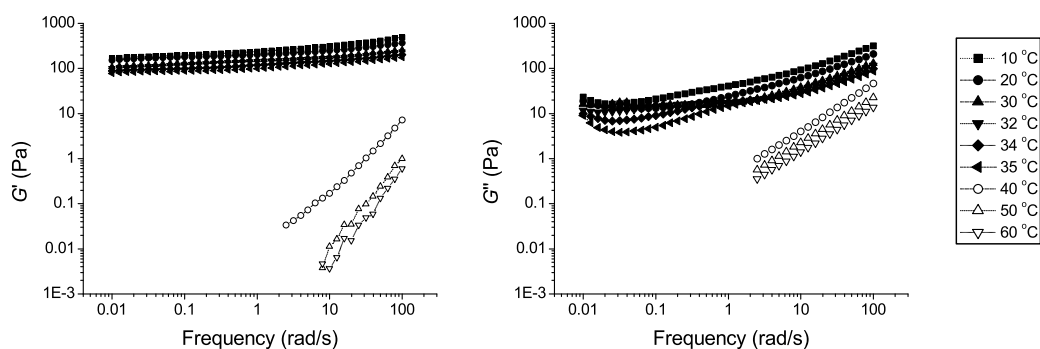


Figure 5.33: Dynamic storage modulus (G') and loss modulus (G'') of 10 wt % 620(80)AB diblock in 5CB. The mixture is single-phase nematic for all $T \leq 35.5$ °C (closed symbols) and single-phase isotropic for $T \geq 40.0$ °C (open symbols).

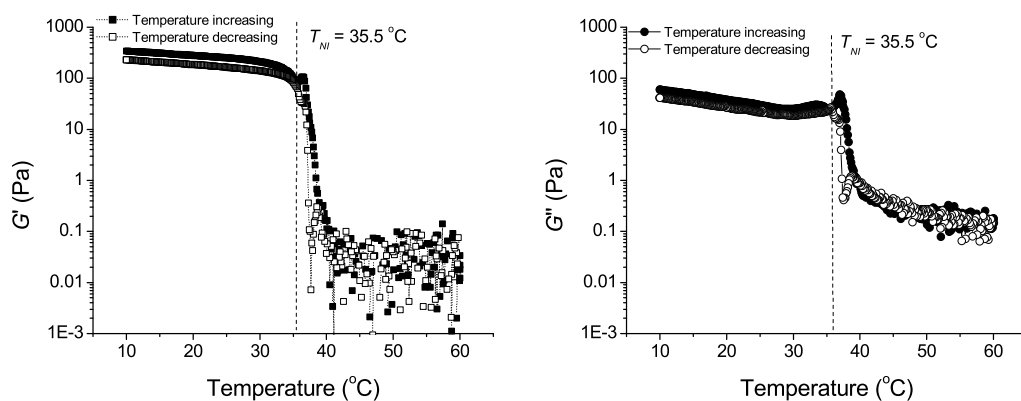


Figure 5.34: Dynamic storage modulus (G') and loss modulus (G'') of 10 wt % 620(80) AB diblock in 5CB while heating (closed symbols) and cooling (open symbols) at 0.5 °C/min

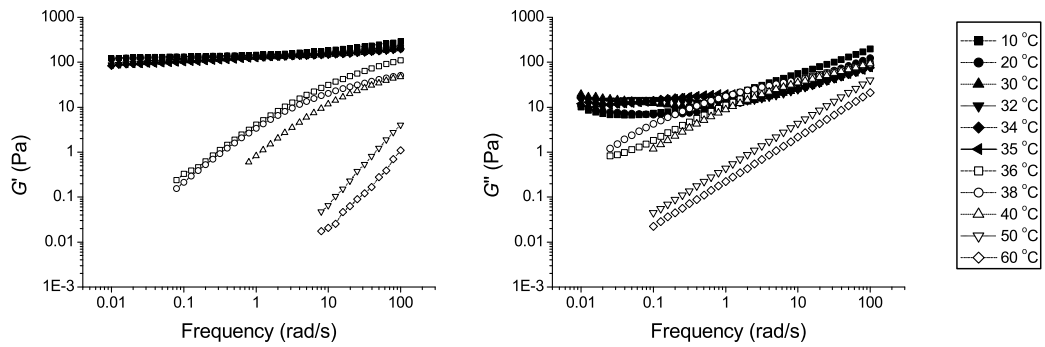


Figure 5.35: Dynamic storage modulus (G') and loss modulus (G'') of 10 wt % 450(120) AB diblock in 5CB. The mixture is single-phase nematic for all $T < 36.0$ °C (closed symbols) and single-phase isotropic for $T \geq 36.0$ °C (open symbols).

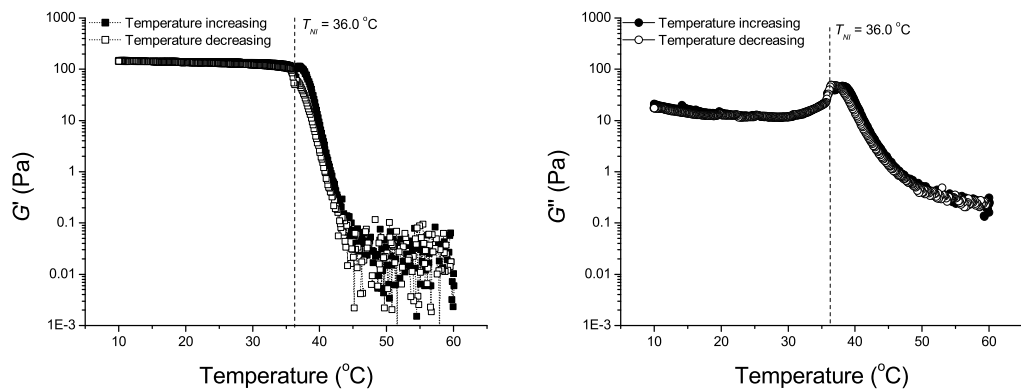


Figure 5.36: Dynamic storage modulus (G') and loss modulus (G'') of 10 wt % 450(120) AB diblock in 5CB while heating (closed symbols) and cooling (open symbols) at 0.5 °C/min

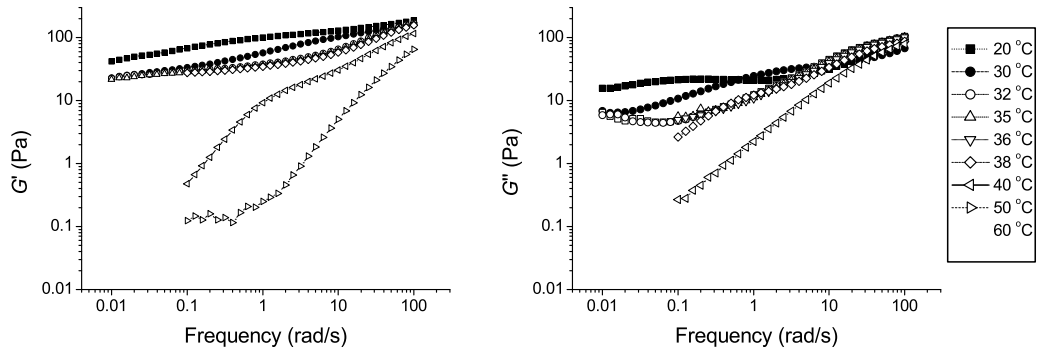


Figure 5.37: Dynamic storage modulus (G') and loss modulus (G'') of 10 wt % 840(190) AB diblock in 5CB. The mixture is single-phase nematic for all $T \leq 31.8$ °C (closed symbols) and single-phase isotropic for $T \geq 34.0$ °C (open symbols).

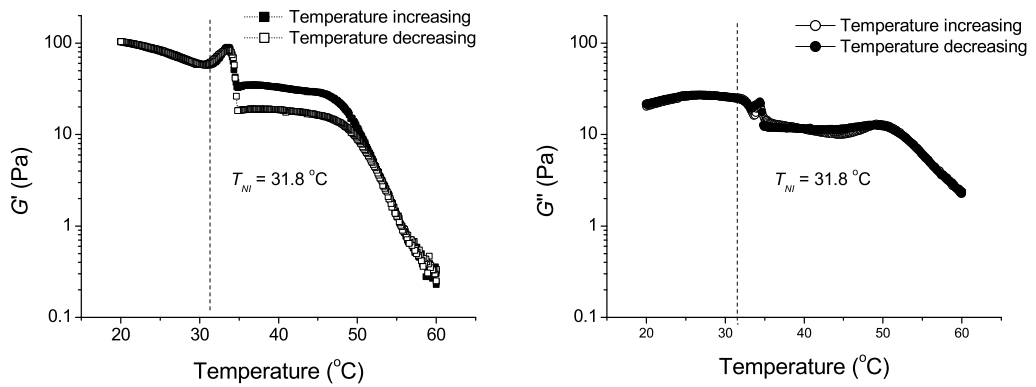


Figure 5.38: Dynamic storage modulus (G') and loss modulus (G'') of 10 wt % 840(190) AB diblock in 5CB while heating (closed symbols) and cooling (open symbols) at 0.5 °C/min

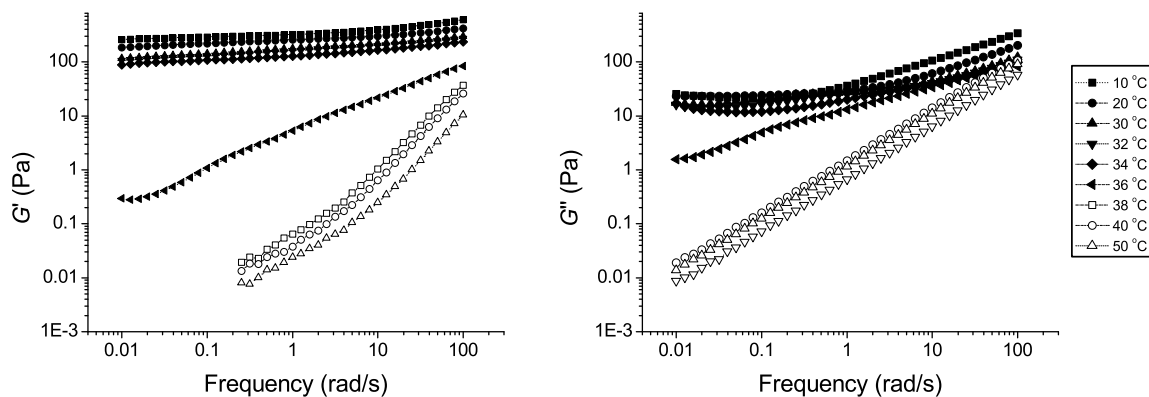


Figure 5.39: Dynamic storage modulus (G') and loss modulus (G'') of 10 wt % 1320(60) ABA triblock in 5CB. The mixture is single-phase nematic for all $T \leq 37.0$ °C (closed symbols) and single-phase isotropic for $T > 37.0$ °C (open symbols). The experiments were performed with a parallel-plate fixture with a gap of 500 μm .

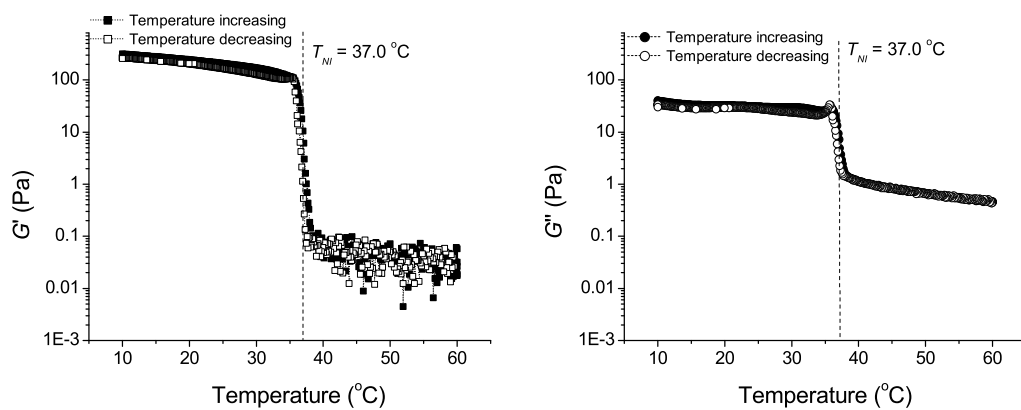


Figure 5.40: Dynamic storage modulus (G') and loss modulus (G'') of 10 wt % 1320(60) ABA triblock in 5CB while heating (closed symbols) and cooling (open symbols) at 0.5 °C/min. The experiments were performed with a parallel-plate fixture with a gap of 500 μm .

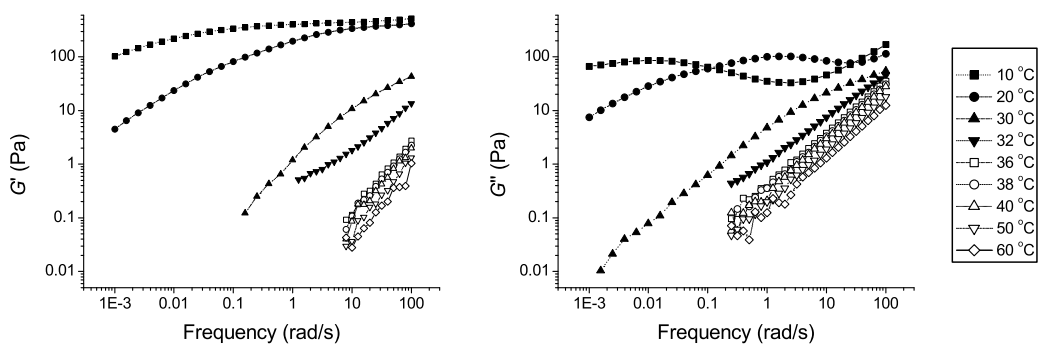


Figure 5.41: Dynamic storage modulus (G') and loss modulus (G'') of 10 wt % 800(20) ABA triblock in 5CB. The mixture is single-phase nematic for all $T \leq 32.0$ °C (closed symbols) and single-phase isotropic for $T \geq 35.7$ °C (open symbols).

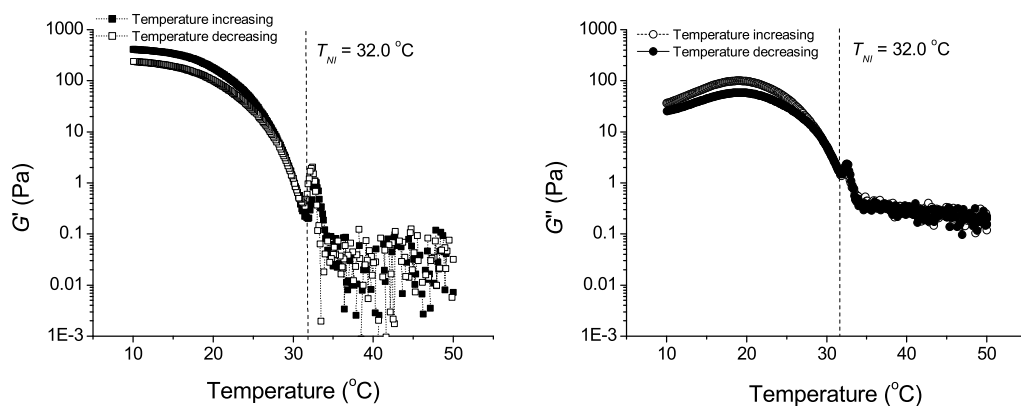


Figure 5.42: Dynamic storage modulus (G') and loss modulus (G'') of 10 wt % 800(20) ABA triblock in 5CB while heating (closed symbols) and cooling (open symbols) at 0.5 °C/min

Bibliography

- [1] Z. Ergundor, C. W. Manke, and E. Gulari. Atomization and elongational viscosity of associating triblock copolymer solutions. *J. Non-Newtonian Fluid Mech.*, 97(2-3):159–167, 2001.
- [2] W. Shen, R. G. H. Lammertink, J. K. Sakata, J. A. Kornfield, and D. A. Tirrell. Assembly of an artificial protein hydrogel through leucine zipper aggregation and disulfide bond formation. *Macromolecules*, 38(9):3909–3916, 2005.
- [3] H. Hori, O. Urakawa, and K. Adachi. Dielectric relaxation in phase-segregated mixtures of polystyrene and liquid crystal 5cb. *Macromolecules*, 37:1583–1590, 2004.
- [4] S. T. Wu, Q. H. Wang, M. D. Kempe, and J. A. Kornfield. Perdeuterated cyanobiphenyl liquid crystals for infrared applications. *J. Appl. Phys.*, 92(12):7146–7148, 2002.
- [5] M. D. Kempe, N. R. Scruggs, R. Verduzco, J. Lal, and J. A. Kornfield. Self-assembled liquid-crystalline gels designed from the bottom up. *Nat. Mater.*, 3(3):177–182, 2004.
- [6] M. Walther, H. Faulhammer, and H. Finkelmann. On the thread-like morphology of lc/i block copolymers in nematic solvents. *Macromol. Chem. Phys.*, 199:223–237, 1998.
- [7] N. Leroux, P. Keller, M. F. Achard, L. Noirez, and F. Hardouin. Small angle neutron scattering experiments on “side-on fixed” liquid crystal polyacrylates. *J. Phys. II France*, 3:1289–1296, 1993.
- [8] S. Lecommandoux, M. F. Achard, F. Hardouin, A. Brulet, and J. P. Cotton. Are nematic side-on polymers totally extended? a sans study. *Liq. Cryst.*, 22(5):549–555, 1997.

- [9] M. H. Li, A. Brulet, P. Davidson, P. Keller, and J. P. Cotton. Observation of hairpin defects in a nematic main-chain polyester. *Phys. Rev. Lett.*, 70(15):2297–2300, 1993.
- [10] G. A. McConnell, A. P. Gast, J. S. Huang, and S. D. Smith. Disorder-order transitions in soft sphere polymer micelles. *Phys. Rev. Lett.*, 71(13):2102–2105, 1993.
- [11] I. W. Hamley, J. P. A. Fairclough, A. J. Ryan, C. Y. Ryu, T. P. Lodge, A. J. Gleeson, and J. S. Pedersen. Micellar ordering in concentrated solutions of di- and triblock copolymers in a slightly selective solvent. *Macromolecules*, 31:1188–1196, 1998.
- [12] J. S. Higgins, S. Blake, P. E. Tomlins, S. B. Ross-Murphy, E. Staples, J. Penfold, and J. V. Dawkins. Comparison of the structural and rheological consequences of micelle formation in solutions of a model di-block copolymer. *Polymer*, 29:1968–1978, 1988.
- [13] I. W. Hamley. Amphiphilic diblock copolymer gels: the relationship between structure and rheology. *Phil. Trans. R. Soc. Lon. A*, 359:1017–1044, 2001.
- [14] J. S. Pedersen. Analysis of small-angle scattering data from colloids and polymer solutions: modeling and least-squares fitting. *Adv. Colloid Interface Sci.*, 70:171–210, 1997.
- [15] Kell Mortensen. Structural studies of aqueous solutions of peo-ppo-peo triblock copolymers, their micellar aggregates and mesophases; a small-angle neutron scattering study. *J. Phys.: Condens. Matter*, 8:A103–A124, 1996.
- [16] T. P. Lodge, Joona Bang, Moon Jeong Park, and Kookheon Char. Origin of the thermoreversible fcc-bcc transition in block copolymer solutions. *Phys. Rev. Lett.*, 92(14):145501, 2004.
- [17] T. P. Lodge, X. Xu, C. Y. Ryu, I. W. Hamley, J. P. A. Fairclough, A. J. Ryan, and J. S. Pedersen. Structure and dynamics of concentrated solutions of asymmetric block copolymers in slightly selective solvents. *Macromolecules*, 29:5955–5964, 1996.
- [18] F. S. Bates, J. H. Rosedale, and G. H. Freckrickson. Fluctuation effects in a symmetric diblock copolymer near the order-disorder transition. *Macromolecules*, 92(10):6255–6270, 1990.

- [19] N. R. Scruggs. PhD thesis, California Institute of Technology, 2007.
- [20] G. Holden, E. T. Bishop, and N. R. Legge. Thermoplastic elastomers. *J. Polym. Sci., Part C: Polym. Sym.*, page 37, 1969.
- [21] K. Almdal, J. Dyre, S. Hvidt, and O. Kramer. What is a gel? *Makromol. Chem., Macromol. Sym.*, 76:49–51, 1993.
- [22] H. Li, G.-E. Yu, C. Price, and C. Booth. Concentrated aqueous micellar solutions of diblock copoly(oxyethylene/oxybutylene) $e_{41}b_8$: A study of phase behavior. *Macromolecules*, 30:1347–1354, 1997.
- [23] H. Watanabe, S. Kuwahara, and T. Kotaka. Rheology of styrene-butadiene-styrene triblock copolymer in *n*-tetradecane systems. *J. Rheol.*, 28(4):393–409, 1984.
- [24] N. R. Scruggs, J. A. Kornfield, and J. Lal. Using the “switchable” quality of liquid crystal solvents to mediate segregation between coil and liquid crystalline polymers. *Macromolecules*, 39(11):3921–3926, 2006.
- [25] A. Halperin, M. Tirrell, and T. P. Lodge. Tethered chains in polymer microstructures. *Adv. Polym. Sci.*, 100:31–71, 1992.